ACS OMEGA

http://pubs.acs.org/journal/acsodf

Article

Influence of Ag Clusters on the Electronic Structures of β-Ga_2O_3 Photocatalyst Surfaces

Muneaki Yamamoto,* Akihide Kuwabara, and Tomoko Yoshida*

Cite This: *ACS Omega* 2021, 6, 33701−33707

Read Online

ACCESS | Metrics & More | Article Recommendations | Supporting Information

ABSTRACT: In order to understand the photocatalytic carbon dioxide reduction over Ag-loaded β-Ga_2O_3 photocatalysts, first principles calculations based on density functional theory were performed on the surface model of a Ag cluster-adsorbed β-Ga_2O_3 system. The stable adsorption structures of Ag_n (n = 1 to 4) clusters on the β-Ga_2O_3 (100) surface were determined. In the electronic structure analysis, the valence states of all Ag clusters mixed with the top of the O 2p valence band of Ga_2O_3, leading the Fermi level of Ag_n/β-Ga_2O_3 to shift to the bottom of the conduction band. It was also revealed that the unoccupied states of Ag_n clusters overlapped with the Ga unoccupied states, and occupied electronic states of Ag clusters were formed in the band gap. These calculation results corresponded to the experimental ones obtained in our previous study, i.e., small Ag clusters had strong interaction with the Ga_2O_3 surface, enhancing the electron transfer between the Ag clusters and the Ga_2O_3 surface. That is, excited electrons toward Ag_n clusters or the perimeter of Ag-Ga_2O_3 should be the important key to promote photocatalytic CO_2 reduction.

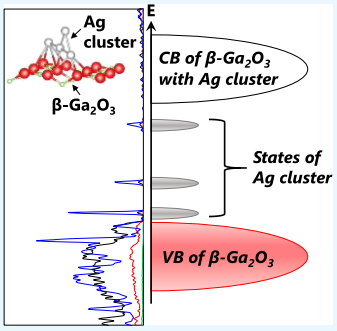

1. INTRODUCTION

Photocatalytic reduction of carbon dioxide by semiconductor photocatalysts is drawing much attention as one of the solutions to environmental and energy problems, because carbon dioxide as a causative substance of global warming can be recycled by solar energy.[1−6] From the viewpoint of realizing artificial photosynthesis, it is important to develop a material that can accelerate the carbon dioxide reduction reaction in water using water as the electron source.

Since the reduction of carbon dioxide in water competes with the reduction of protons in water, which is thermodynamically favorable, it is necessary to promote the carbon dioxide reduction by loading an appropriate cocatalyst on the surface of a semiconductor photocatalyst. In general, cocatalysts are considered to have the function of providing reaction sites and reducing the activation energy of the reaction and also promoting the charge separation of the electrons and holes generated in the semiconductor by light.[5,6] Previous studies have reported that the activity and the selectivity of the carbon dioxide reduction reaction is improved when silver is loaded as a cocatalyst on semiconductor photocatalysts.[7−15]

Among semiconductor photocatalysts, β-gallium oxide (β-Ga_2O_3) is known to be a highly active semiconductor photocatalyst for overall water splitting.[16] It has been also reported that β-Ga_2O_3 exhibits activity for reduction of carbon dioxide in water with a silver cocatalyst.[10,11] In our previous research, the adsorption behavior of carbon dioxide on silver-loaded β-Ga_2O_3 (Ag/β-Ga_2O_3) was observed by in situ FT-IR measurement, and we have found that silver clusters promote the formation of the intermediates in the carbon dioxide reduction reaction.[11] However, it is not clear how silver clusters on β-Ga_2O_3 work and promote the reduction of carbon dioxide. It is experimentally difficult to investigate the local structure and electronic states of minute reaction sites created by extremely small metal clusters and metal oxide surfaces.

In order to clarify the physical and chemical properties of such surface reaction sites and to understand the photocatalytic reaction mechanism, theoretical research using first principles calculations will be a powerful technique. For example, the first principles electronic structure calculations were performed on metallic nickel and nickel oxide-loaded β-Ga_2O_3 (Ni−NiO/β-Ga_2O_3) photocatalytic systems, and it was suggested that metallic nickel contributes to the hydrogen evolution reaction in the overall water splitting and nickel oxide would take part in the oxygen evolution reaction.[17] However, as far as we know, first principles calculations were not performed on the surface model of the Ag cluster/β-Ga_2O_3 system.

In this study, in order to understand the photocatalytic carbon dioxide reduction over the Ag/β-Ga_2O_3 photocatalyst, first principles calculations were performed on the surface model of the Ag cluster/β-Ga_2O_3 system for the first time. It

Received: August 30, 2021
Accepted: November 23, 2021
Published: December 3, 2021

https://doi.org/10.1021/acsomega.1c04730
ACS Omega 2021, 6, 33701−33707

has been reported that the (100) plane is the most stable in β-Ga_2O_3,[17,18] thus we chose the β-Ga_2O_3 (100) surface. In this study, the surface structure and surface energy were calculated for two different types of termination of β-Ga_2O_3 (100) surfaces. Ag_n (n = 1 to 4) clusters were adsorbed to the stable surface, and the most stable adsorption structure was determined. Furthermore, we examined the density of states (DOS) and the spatial distribution of wave functions for the Ag_n/β-Ga_2O_3 system. DOS is a powerful tool to analyze the energy levels of the system. The region between the top of the valence band and the bottom of the conduction band are similar to the HOMO and LUMO, which are related to the photocatalytic reactivity of Ag/β-Ga_2O_3.[19,20]

2. RESULTS AND DISCUSSION

First, structural optimization was performed for the unit cell of β-Ga_2O_3 (the left of Figure 1). As a result, lattice constants a, b, c and lattice angle β were calculated to be 12.42, 3.09, 5.88 Å and 103.74°, respectively. These values are almost the same as previously reported calculation results and in good agreement with the experimental result.[17,21]

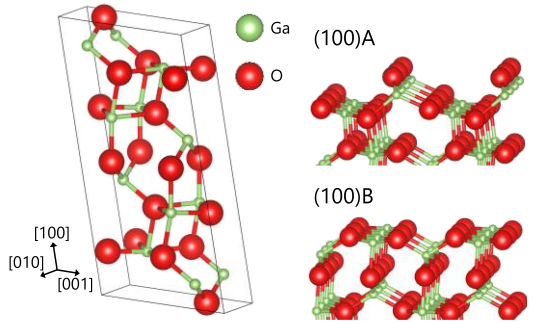

Figure 1. Unit cell of β-Ga_2O_3 and (100) surface models with different types of termination.

Structural optimization and surface energy calculations of a β-Ga_2O_3 (100) surface were carried out for two different terminations of the (100) plane. One of the termination referred to as (100)A is shown in the upper right of Figure 1 and the other denoted as (100)B is represented in the lower right of Figure 1. The surface energy γ was calculated by the following equation:

$$\gamma = (E_{slab} - nE_{perf})/2S$$

where E_{slab} is the total energy of the surface slab model, E_{perf} is the total energy of the unit cell, n is the number of Ga_2O_3 units included in the surface slab model, and S is the surface area of the surface slab model.

The surface energies are summarized in Table 1. The (100)B surface was more stable than the (100)A surface. The values of the surface energy were almost the same between 8 and 12 atomic layers with the difference within 0.01 J/m^2. Therefore, we assumed that the surface energy sufficiently converged at 12 layers.

Table 1. Surface Energies of Different Numbers of Atomic Layers and Termination Types of the β-Ga_2O_3 (100) Surface

slab	surface energy [J/m^2]
(100)A−8 layers	0.783
(100)A−12 layers	0.779
(100)B−8 layers	0.457
(100)B−12 layers	0.449

Subsequently, the (100)B surface with 12 atomic layers was expanded to (3 × 2) to make the surface model where the Ag_n (n = 1 to 4) cluster was adsorbed. The adsorption energy of the Ag_n cluster $E_{ad}(n)$ was calculated by the following equation:

$$E_{ad}(n) = E_{slab+Ag}(n) - E_{slab} - E_{Ag}(n)$$

where $E_{slab\ +\ Ag}(n)$ is the total energy of the Ag_n cluster-adsorbed β-Ga_2O_3 (100) surface slab model, E_{slab} is the total energy of the bare β-Ga_2O_3 (100) surface slab model, and $E_{Ag}(n)$ is the is the total energy of the optimized Ag_n cluster in a vacuum.

First, the Ag_1 cluster was arranged at six different adsorption sites on the β-Ga_2O_3 (100) surface as initial conditions as shown in Figure 2. Figure S1 shows the structures of the Ag_1/β-Ga_2O_3 (100) surface after optimization for each initial conditions. Bonds are drawn between atoms within a distance of 3.5 Å. The relative energies with respect to the most stable surface and the adsorption energies of the Ag_1 cluster are summarized in Table S1.

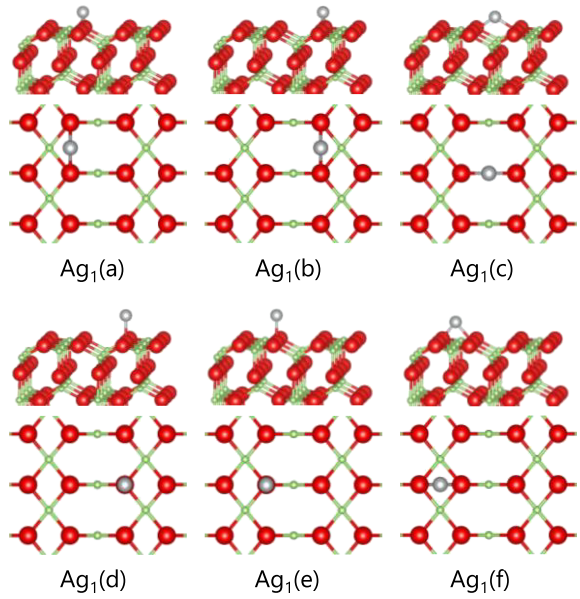

Figure 2. Side (upper) and top (lower) views of structures of the Ag_1/β-Ga_2O_3 (100) surface at different sites as initial conditions.

For the case of $n \geq 2$, initial structures of Ag_n/β-Ga_2O_3 (100) were constructed by adding a Ag atom on one of the possible adsorption sites near the Ag_{n-1} cluster of the most stable configuration of the Ag_{n-1}/β-Ga_2O_3 (100) models. Results of optimized structures and adsorption energies of the Ag_n cluster (n = 2 to 4) on the β-Ga_2O_3 (100) surface are shown in Figures S2−S4 and Tables S2−S4, respectively.

Figure 3 shows the most stable structures of the Ag_n/β-Ga_2O_3 (100) surface (n = 1 to 4). Ag atoms and the O atoms that are the nearest neighbor to the Ag atoms are labeled. By comparing with the adsorption energies of the most stable structures of the Ag_n/β-Ga_2O_3 (100) surface (n = 1 to 4) in Tables S1−S4, we found that the adsorption energy tends to become less negative with increasing of Ag atoms while odd

https://doi.org/10.1021/acsomega.1c04730
ACS Omega 2021, 6, 33701−33707

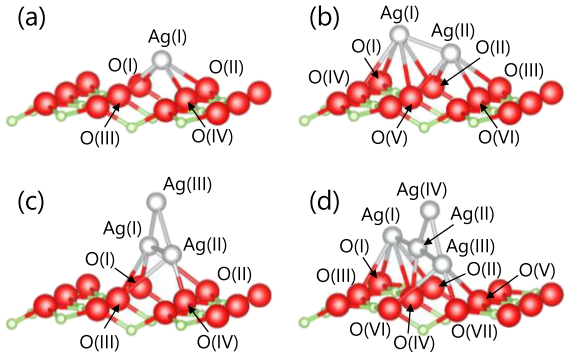

Figure 3. Most stable structures of the Ag_n/β-Ga_2O_3 (100) surface. (a) n = 1, (b) n = 2, (c) n = 3, and (d) n = 4.

number clusters (Ag_1 or Ag_3) were more stable, suggesting the Ag cluster size dependence of the adsorption energy.[22]

Tables 2345 summarize the bond lengths in the Ag_n/β-Ga_2O_3 (100) surfaces. The most stable adsorption site for an isolated Ag atom (Figure 3a) is a hollow site in the middle of four nearest O atoms with an adsorption energy of −0.694 eV (Ag_1(a) in Table S1), resulting in four Ag−O bonds with a bond length of 2.681−2.753 Å. When a Ag_2 dimer is adsorbed on the Ga_2O_3 (100) surface, the most energetically favorable structure (Figure 3b) consists of a Ag−Ag bond with a length of 2.644 Å and eight Ag−O bonds of 2.875−3.353 Å. These Ag−O bonds are longer than the Ag−O bond length in the Ag_1/β-Ga_2O_3 (100) surface, suggesting that the formation of the Ag−Ag bond results in the increase of the Ag−O bond length. The adsorption energy of the Ag dimer structure is calculated to be −0.452 eV (Ag_2(a) in Table S2), less stable than the adsorption energy of the isolated Ag atom by 0.242 eV. It can be supposed that the weaker adsorption of the Ag dimer on the β-Ga_2O_3 surface results in longer Ag−O bond distances.[23]

As for the lowest energy structure of the Ag_3/Ga_2O_3 (100) surface (Figure 3c), the adsorption energy is calculated to be −1.654 eV (Ag_3(a) in Table S3), suggesting the strong adsorption of the Ag trimer on Ga_2O_3. Three Ag−Ag bond lengths are evaluated as 2.660−2.711 Å, which are almost equivalent to those in the Ag_2/β-Ga_2O_3 (100) surface. On the other hand, two shorter and three longer Ag−O bonds are found and the corresponding lengths are 2.269−2.277 Å and 3.339−3.453 Å, respectively. The short Ag−O bonds would be involved in the strong adsorption of the Ag trimer on Ga_2O_3.

The introduction of the extra Ag atom to the Ag trimer on Ga_2O_3 suppresses the adsorption energy to −1.089 eV (Ag_4(a) in Table S4) compared to the adsorbed state of the Ag trimer. Investigating the lowest energy structures shown in Figure 3c,d , the difference in Ag−Ag bond lengths is small. On the other hand, the number ratio of two short Ag−O bonds of 2.328−2.478 Å to six long Ag−O bonds of 3.193−3.445 Å in Figure 3d is 1/3, which is less than 2/5, calculated with the number of short and long Ag−O bonds in Figure 3c. The lower ratio of the short Ag−O bond would be related to the less stable adsorption of the Ag_4 cluster compared to the Ag_3 cluster.

Total DOS (TDOS) and projected partial DOS (PDOS) of Ag_n/β-Ga_2O_3 (100) systems are shown in Figure 4. In the graph, the energy at the upper end of the valence band of the β-Ga_2O_3 slab is set to 0 eV. The valence states of all Ag clusters mixed with the top of the O 2p valence band of Ga_2O_3, leading the Fermi level of Ag_n/β-Ga_2O_3 to shift to the bottom of the conduction band.[23] Furthermore, the obvious occupied states of Ag clusters are generated between the band gap of Ga_2O_3, and they increase with the number of Ag atoms. On the other hand, the unoccupied states of Ag_n clusters overlapped with the Ga unoccupied 4s and 4p states. Under photoexcitation, electrons from the O occupied states move to the Ga unoccupied state. Since the Ga unoccupied states overlap with the unoccupied Ag states, the excited electrons generated in the Ga_2O_3 photocatalyst can transfer to Ag.[17] Table 6 summarizes some essential values for each surface model.

Table 2. Bond Length between Silver−Silver or Silver−Neighboring Oxygen of the Ag_1/β-Ga_2O_3 (100) Surface

bond	length [Å]
Ag(I)−O(I)	2.682
Ag(I)−O(II)	2.751
Ag(I)−O(III)	2.681
Ag(I)−O(IV)	2.753

Table 3. Bond Length between Silver−Silver or Silver−Neighboring Oxygen of the Ag_2/β-Ga_2O_3 (100) Surface

bond	length [Å]
Ag(I)−Ag(II)	2.644
Ag(I)−O(I)	3.353
Ag(I)−O(II)	3.300
Ag(I)−O(IV)	3.361
Ag(I)−O(V)	3.295
Ag(II)−O(II)	2.880
Ag(II)−O(III)	3.029
Ag(II)−O(V)	2.875
Ag(II)−O(VI)	3.017

Table 4. Bond Length between Silver−Silver or Silver−Neighboring Oxygen of the Ag_3/β-Ga_2O_3 (100) Surface

bond	length [Å]
Ag(I)−Ag(II)	2.711
Ag(I)−Ag(III)	2.668
Ag(II)−Ag(III)	2.660
Ag(I)−O(I)	2.277
Ag(I)−O(II)	3.453
Ag(I)−O(III)	3.341
Ag(II)−O(III)	3.339
Ag(II)−O(IV)	2.269

Table 5. Bond Length between Silver−Silver or Silver−Neighboring Oxygen of the Ag_4/β-Ga_2O_3 (100) Surface

bond	length [Å]
Ag(I)−Ag(II)	2.695
Ag(II)−Ag(III)	2.813
Ag(II)−Ag(IV)	2.681
Ag(III)−Ag(IV)	2.629
Ag(I)−O(I)	3.193
Ag(I)−O(II)	3.362
Ag(I)−O(III)	3.275
Ag(I)−O(IV)	3.445
Ag(II)−O(IV)	2.478
Ag(III)−O(V)	3.324
Ag(III)−O(VI)	3.227
Ag(III)−O(VII)	2.328

https://doi.org/10.1021/acsomega.1c04730
ACS Omega 2021, 6, 33701−33707

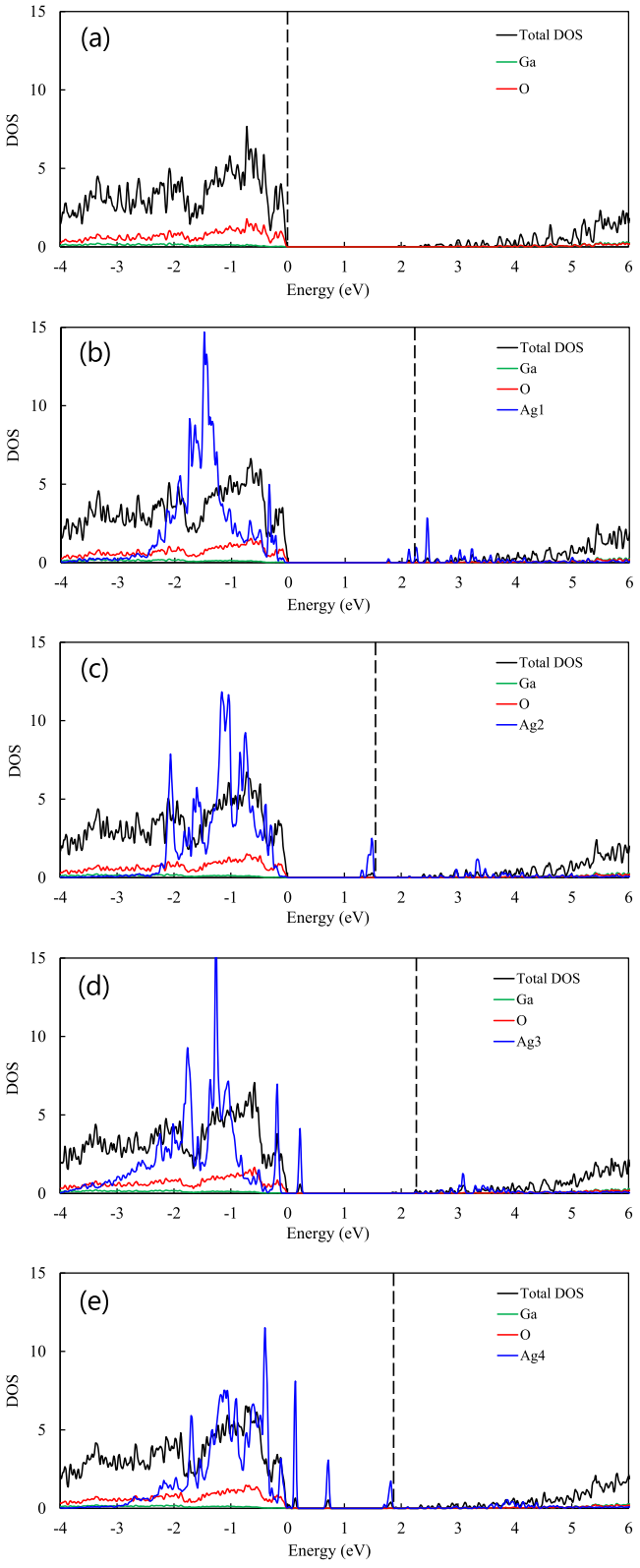

Figure 4. DOS of the bare and Ag-adsorbed β-Ga_2O_3 (100) surface models. (a) β-Ga_2O_3, (b) Ag_1/β-Ga_2O_3, (c) Ag_2/β-Ga_2O_3, (d) Ag_3/β-Ga_2O_3, and (e) Ag_4/β-Ga_2O_3. Fermi levels are represented by dashed lines.

In Figure 5, we visualize spatial distribution of the electronic states by the isosurfaces at 0.005 $Å^{-3}$ of the norm of the wave functions with the energy range from the Fermi level to the energy state 0.5 eV below the Fermi level. As shown in the figure, the highest valence bands are relatively localized on Ag_1, Ag_2, and Ag_4 clusters while they extend to the Ga_2O_3 surface in the Ag_3/β-Ga_2O_3 (100) system. Since the electrons are localized on Ag_1, Ag_2, and Ag_4 clusters, these Ag clusters would be effective CO_2 adsorption sites.[24]

Figure 6 shows isosurfaces of electron probability densities for the localized bands having higher energy states than the valence states, namely, O 2p orbitals, of the β-Ga_2O_3 slab in the Ag_4/β-Ga_2O_3 (100) system. Figure 7 shows the schematic diagram of their band structure of the Ag_4/β-Ga_2O_3 (100) system. In this system, the highest occupied states are localized on the Ag_4 cluster, and the occupied states derived from the Ag_4 cluster would contribute to the local excitation from Ag clusters to the interface between Ag clusters and Ga_2O_3.[25] It should be noted that our calculations based on the density functional theory underestimate the band gap compared to the experiment. The quantitative values of the energy positions of the gap states shown in Figure 7 will be changed if more accurate calculations such as the hybrid density functional ones are performed. However, the characteristics of the chemical bonding between Ga_2O_3 and Ag clusters will remain the same regardless of the formalism of the first principles calculations.

These calculation results correspond to the experimental ones obtained in our previous study,[10,11] i.e., Ag/β-Ga_2O_3 photocatalysts were examined for photocatalytic reduction of CO_2 with water, and the effects of structural and chemical states of the Ag cocatalyst on the photocatalytic reactivity was investigated by studying TEM images, DR UV−vis, and XANES spectra. In particular, Ag L_3-edge XANES and O K-edge XANES spectra suggested a strong interaction between 1 nm sized Ag clusters and the Ga_2O_3 surface, which supports the electron transfer between them. In addition, our in situ FT-IR measurements also revealed that the effective electron transfer can promote the reduction of CO_2 adsorbates to the reaction intermediate species on the perimeter of Ag clusters.

In this study, the electronic structure analyses suggest that the loading of Ag clusters enhances the photocatalytic performance by transferring the excited electrons generated in the Ga_2O_3 photocatalyst to Ag clusters due to the overlap of unoccupied states of Ag_n clusters and Ga as well as the shift of the Fermi level to the conduction band of Ga_2O_3. It was also revealed that occupied electronic states of Ag clusters formed in the band gap may enable local excitation from Ag clusters to the interface between Ag clusters and Ga_2O_3. Excited electrons toward Ag_n clusters or the perimeter of the Ag-Ga_2O_3 interface would be used to reduce CO_2 adsorbates to the reaction intermediate species and which should enhance the photocatalytic performance.

3. CONCLUSIONS

We performed first principles calculations to study the atomic and electronic structures of the Ag_n/β-Ga_2O_3 surface in order to clarify the role of adsorbed Ag_n clusters in the catalysis of carbon dioxide reduction. Surface models of Ag_n/β-Ga_2O_3 (n = 1 to 4) systems were built for first principles electronic structure calculations. The adsorption energy tended to increase with increasing of Ag atoms, while odd number clusters (Ag_1 or Ag_3) were more stable.

In the electronic structure analysis, the valence states of all Ag clusters mixed with the top of the O 2p valence band of Ga_2O_3, leading the Fermi level of Ag_n/β-Ga_2O_3 to shift to the bottom of the conduction band. It was also revealed that the

https://doi.org/10.1021/acsomega.1c04730
ACS Omega 2021, 6, 33701−33707

Table 6. Summary of the Calculation Results for Each Surface Model[a]

surface	adsorption energy of the Ag cluster [eV]	average length of the Ag−Ag bond [Å]	average length of the Ag−O bond [Å]	Fermi level [eV]	energy levels of occupied states of the Ag cluster [eV]		
Ag_1/β-Ga_2O_3	−0.694		2.717	2.227	2.12		
Ag_2/β-Ga_2O_3	−0.452	2.644	3.139	1.581	1.48		
Ag_3/β-Ga_2O_3	−1.654	2.680	2.936	2.262	0.22		
Ag_4/β-Ga_2O_3	−1.089	2.705	3.079	1.858	0.14	0.72	1.82

[a]Fermi levels and energy levels of occupied states of Ag clusters are relative to the valence band maximum level of β-Ga_2O_3.

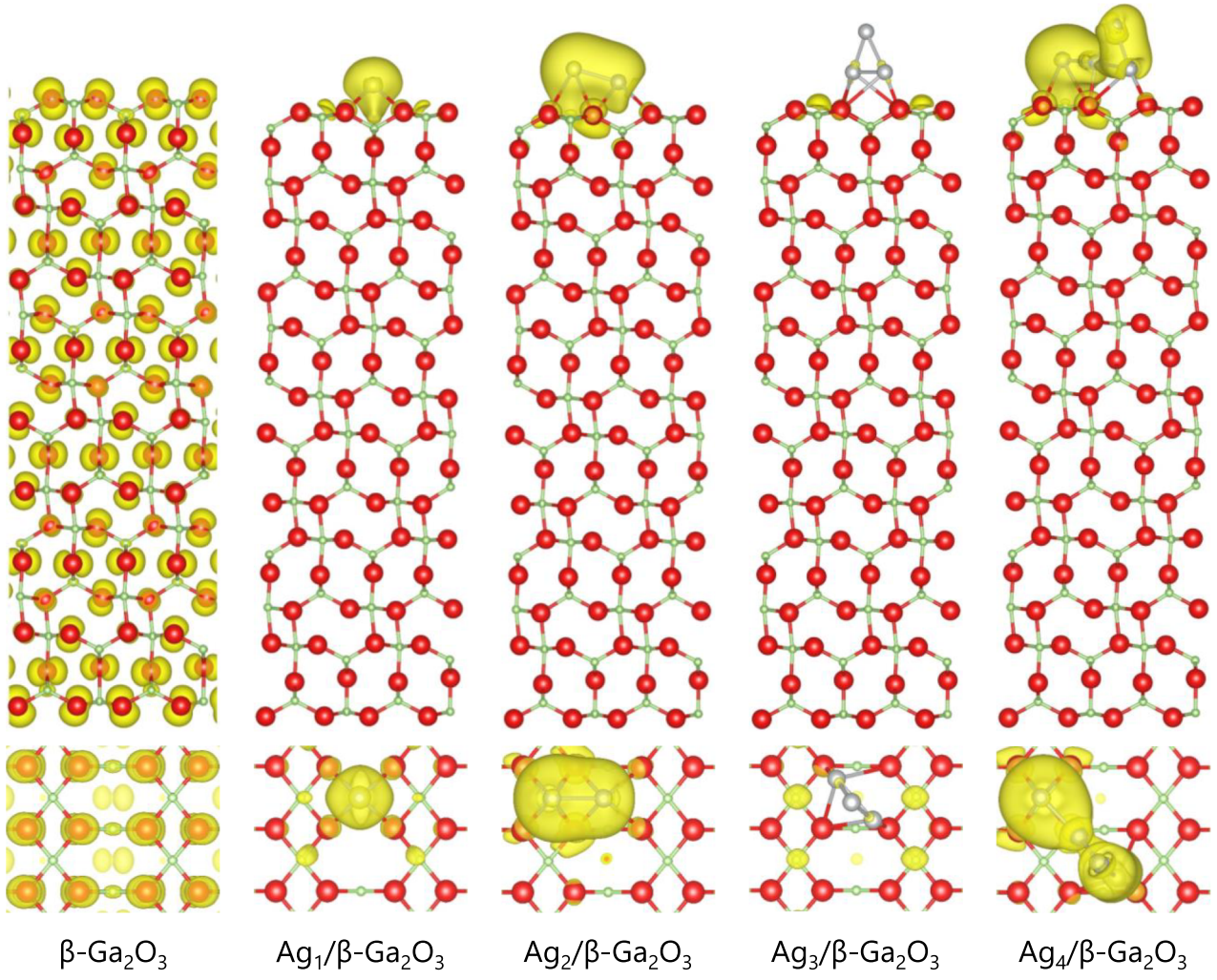

Figure 5. Side (upper) and top (lower) views of the charge density isosurface for the energy level between the Fermi energy and the energy −0.5 eV below from the Fermi energy of the Ag_n/β-Ga_2O_3 (100) system.

unoccupied states of Ag_n clusters overlapped with the Ga unoccupied states. Therefore, the excited electrons generated in the Ga_2O_3 photocatalyst can transfer to Ag efficiently. Regarding Ag_4/β-Ga_2O_3, occupied states derived from Ag_4 clusters were formed in the band gap and right above the valence band of β-Ga_2O_3, which may enable local excitation from Ag clusters to the interface between Ag clusters and Ga_2O_3. These calculation results suggest the loading of Ag clusters would enhance the photocatalytic performance, corresponding to the experimental fact that Ga_2O_3 with small Ag clusters showed high activity for CO_2 reduction.

4. CALCULATION METHODS

We obtain total energies and energy-minimized configurations using first principles calculations based on the plane-wave basis sets and the projector augmented wave method[26] implemented in the VASP code.[27] The Perdew−Burke−Ernzerhof generalized gradient approximation (PBE-GGA) is used for the exchange-correlation functional.[28] For all calculations, the cutoff energy of the plane waves was set to be at 500 eV. Structure optimization calculations were performed until all forces acting on atoms of calculated structure models were less

https://doi.org/10.1021/acsomega.1c04730
ACS Omega 2021, 6, 33701−33707

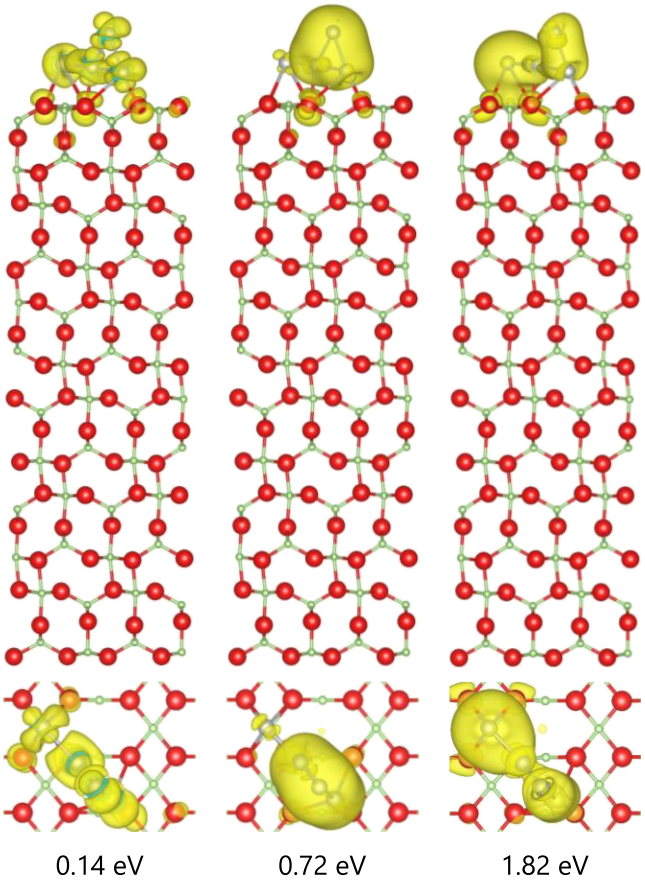

Figure 6. Side (upper) and top (lower) views of the charge density isosurface for the internal band between the band gap of the Ag_4/β-Ga_2O_3 (100) system. Relative energies from the valence band maximum level of β-Ga_2O_3 are written at the bottom of each graph.

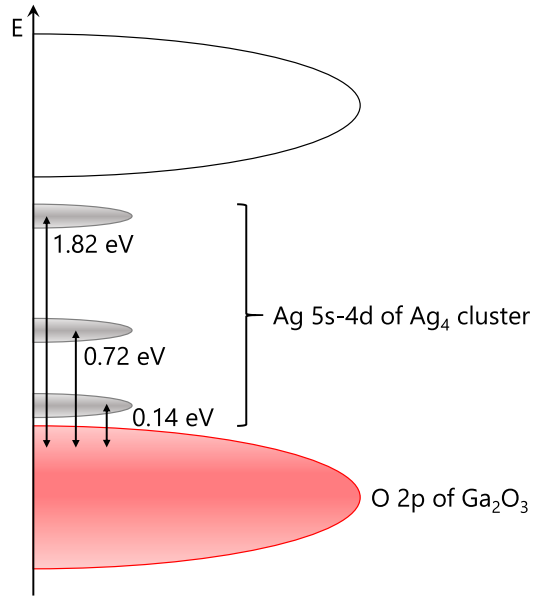

Figure 7. Schematic diagram of the band structure of the Ag_4/β-Ga_2O_3 (100) system.

than 0.02 eV/Å. The valence electron configurations are $3d^{10}$ $4s^2$ $4p^1$ for gallium, $2s^2$ $2p^4$ for oxygen, and $4d^{10}$ $5s^1$ for silver.

The calculation of the β-Ga_2O_3 unit cell was performed with $2 \times 6 \times 4$ k-point meshes of the Brillouin zone sampling based on the Monkhorst-Pack scheme.[29] A surface slab model was used for calculations of the β-Ga_2O_3 (100) surface. A (1×1) slab model containing 8 or 12 atomic layers in the (100) direction with a 20 Å vacuum spacing was constructed from the optimized β-Ga_2O_3 unit cell. For the calculation of the surface where the Ag_n cluster (n = 1 to 4) was adsorbed, (3×2) supercells of the surface slab model were constructed. The mesh sizes of the Brillouin zone sampling were $6 \times 4 \times 1$ and $2 \times 2 \times 1$ in the clean surface model and the Ag-absorbed surface model, respectively. The two of the central atomic layers of Ga_2O_3 were fixed for all surface slab model calculations. The energy of isolated Ag_n clusters in vacuum was used to calculate the adsorption energy of Ag_n clusters. In this study, all crystal and surface models are visualized by VESTA.[30]

■ ASSOCIATED CONTENT

Supporting Information

The Supporting Information is available free of charge at https://pubs.acs.org/doi/10.1021/acsomega.1c04730.

Views of optimized structures of the Ag_{1-4}/β-Ga_2O_3 (100) surface at different sites and their relative energies and adsorption energies (PDF)

■ AUTHOR INFORMATION

Corresponding Authors

Muneaki Yamamoto − *Research Center for Artificial Photosynthesis, Osaka City University, Osaka 558-8585, Japan;* orcid.org/0000-0003-2076-2419; Email: m-yamamoto@osaka-cu.ac.jp

Tomoko Yoshida − *Research Center for Artificial Photosynthesis, Osaka City University, Osaka 558-8585, Japan;* orcid.org/0000-0003-2117-5400; Email: tyoshida@osaka-cu.ac.jp

Author

Akihide Kuwabara − *Nanostructures Research Laboratory, Japan Fine Ceramics Center, Nagoya 456-8587, Japan;* orcid.org/0000-0002-2810-3437

Complete contact information is available at: https://pubs.acs.org/10.1021/acsomega.1c04730

Notes

The authors declare no competing financial interest.

■ ACKNOWLEDGMENTS

This study was supported by JSPS KAKENHI Grant Number JP16H06440 (Synthesis of Mixed Anion Compounds toward Novel Functionalities).

■ REFERENCES

(1) Kubacka, A.; Fernández-García, M.; Colón, G. Advanced Nanoarchitectures for Solar Photocatalytic Applications. *Chem. Rev.* **2012**, *112*, 1555−1614.

(2) Habisreutinger, S. N.; Schmidt-Mende, L.; Stolarczyk, J. K. Photocatalytic Reduction of CO_2 on TiO_2 and Other Semiconductors. *Angew. Chem., Int. Ed.* **2013**, *52*, 7372−7408.

(3) White, J. L.; Baruch, M. F.; Pander, J. E., III; Hu, Y.; Fortmeyer, I. C.; Park, J. E.; Zhang, T.; Liao, K.; Gu, J.; Yan, Y.; Shaw, T. W.; Abelev, E.; Bocarsly, A. B. Light-Driven Heterogeneous Reduction of Carbon Dioxide: Photocatalysts and Photoelectrodes. *Chem. Rev.* **2015**, *115*, 12888−12935.

(4) Li, K.; Peng, B.; Peng, T. Recent Advances in Heterogeneous Photocatalytic CO_2 Conversion to Solar Fuels. *ACS Catal.* **2016**, *6*, 7485−7527.
(5) Ran, J.; Jaroniec, M.; Qiao, S. Z. Cocatalysts in Semiconductor-based Photocatalytic CO_2 Reduction: Achievements, Challenges, and Opportunities. *Adv. Mater.* **2018**, *30*, No. 1704649.
(6) Li, X.; Yu, J.; Jaroniec, M.; Chen, X. Cocatalysts for Selective Photoreduction of CO_2 into Solar Fuels. *Chem. Rev.* **2019**, *119*, 3962−4179.
(7) Iizuka, K.; Wato, T.; Miseki, Y.; Saito, K.; Kudo, A. Photocatalytic Reduction of Carbon Dioxide over Ag Cocatalyst-Loaded $ALa_4Ti_4O_{15}$ (A = Ca, Sr, and Ba) Using Water as a Reducing Reagent. *J. Am. Chem. Soc.* **2011**, *133*, 20863−20868.
(8) Teramura, K.; Wang, Z.; Hosokawa, S.; Sakata, Y.; Tanaka, T. A Doping Technique that Suppresses Undesirable H_2 Evolution Derived from Overall Water Splitting in the Highly Selective Photocatalytic Conversion of CO_2 in and by Water. *Chem. − Eur. J.* **2014**, *20*, 9906−9909.
(9) Takayama, T.; Tanabe, K.; Saito, K.; Iwase, A.; Kudo, A. The $KCaSrTa_5O_{15}$ Photocatalyst with Tungsten Bronze Structure for Water Splitting and CO_2 Reduction. *Phys. Chem. Chem. Phys.* **2014**, *16*, 24417−24422.
(10) Yamamoto, M.; Yoshida, T.; Yamamoto, N.; Yoshida, H.; Yagi, S. In-Situ FT-IR Study on the Mechanism of CO_2 Reduction with Water over Metal (Ag or Au) Loaded Ga_2O_3 Photocatalysts. *e-J. eJSSNT* **2014**, *12*, 299−303.
(11) Yamamoto, M.; Yoshida, T.; Yamamoto, N.; Nomoto, T.; Yamamoto, Y.; Yagi, S.; Yoshida, H. Photocatalytic Reduction of CO_2 with Water Promoted by Ag Clusters in Ag/Ga_2O_3 Photocatalysts. *J. Mater. Chem. A* **2015**, *3*, 16810−16816.
(12) Zhu, X.; Anzai, A.; Yamamoto, A.; Yoshida, H. Silver-Loaded Sodium Titanate Photocatalysts for Selective Reduction of Carbon Dioxide to Carbon Monoxide with Water. *Appl. Catal. B: Environ.* **2019**, *243*, 47−56.
(13) Zhang, F.; Li, Y. H.; Qi, M. Y.; Tang, Z. R.; Xu, Y. J. Boosting the Activity and Stability of Ag-Cu_2O/ZnO Nanorods for Photocatalytic CO_2 Reduction. *Appl. Catal. B: Environ.* **2020**, *268*, No. 118380.
(14) Wang, S.; Teramura, K.; Asakura, H.; Hosokawa, S.; Tanaka, T. Effect of Zn in Ag-Loaded Zn-Modified $ZnTa_2O_6$ for Photocatalytic Conversion of CO_2 by H_2O. *J. Phys. Chem. C* **2021**, *125*, 1304−1312.
(15) Soltani, T.; Yamamoto, A.; Singh, S. P.; Anzai, A.; Fudo, E.; Tanaka, A.; Kominami, H.; Yoshida, H. Simultaneous Formation of CO and H_2O_2 from CO_2 and H_2O with a $Ag−MnO_x/CaTiO_3$ Photocatalyst. *ACS Appl. Energy Mater.* **2021**, *4*, 6500−6510.
(16) Yanagida, T.; Sakata, Y.; Imamura, H. Photocatalytic Decomposition of H_2O into H_2 and O_2 over Ga_2O_3 Loaded with NiO. *Chem. Lett.* **2004**, *33*, 726−727.
(17) Liu, T.; Tranca, I.; Yang, J.; Zhou, X.; Li, C. Theoretical Insight into the Roles of Cocatalysts in the Ni-NiO/β-Ga_2O_3 Photocatalysts for Overall Water Splitting. *J. Mater. Chem. A* **2015**, *3*, 10309−10319.
(18) Bermudez, V. M. The Structure of Low-index Surfaces of β-Ga_2O_3. *Chem. Phys.* **2006**, *323*, 193−203.
(19) Pacchioni, G. Electronic Interactions and Charge Transfers of Metal Atoms and Clusters on Oxide Surfaces. *Phys. Chem. Chem. Phys.* **2013**, *15*, 1737−1757.
(20) Deng, H.; Yu, Y.; Liu, F.; Ma, J.; Zhang, Y.; He, H. Nature of Ag Species on Ag/γ-Al_2O_3: A Combined Experimental and Theoretical Study. *ACS Catal.* **2014**, *4*, 2776−2784.
(21) Geller, S. Crystal Structure of β-Ga_2O_3. *J. Chem. Phys.* **1960**, *33*, 676−684.
(22) Klacar, S.; Hellman, A.; Panas, I.; Grönbeck, H. Oxidation of Small Silver Clusters: A Density Functional Theory Study. *J. Phys. Chem. C* **2010**, *114*, 12610−12617.
(23) Quyang, T.; Fan, W.; Guo, J.; Zheng, Y.; Yin, X.; Shen, Y. DFT Study on Ag Loaded 2H-MoS_2 for Understanding the Mechanism of Improved Photocatalytic Reduction of CO_2. *Phys. Chem. Chem. Phys.* **2020**, *22*, 10305−10313.
(24) Wan, D.; Liu, Z.; Yang, W. Revealing the Size Effect of Platinum Cocatalyst for Photocatalytic Hydrogen Evolution on TiO_2 Support: A DFT Study. *ACS Catal.* **2018**, *8*, 7270−7278.
(25) Puigdollers, A. R.; Schlexer, P.; Pacchioni, G. Gold and Silver Clusters on TiO_2 and ZrO_2 (101) Surfaces: Role of Dispersion Forces. *J. Phys. Chem. C* **2015**, *119*, 15381−15389.
(26) Blöchl, P. E. Projector Augmented-Wave Method. *Phys. Rev. B* **1994**, *50*, 17953−17979.
(27) Kresse, G.; Furthmüller, J. Efficient Iterative Schemes for *Ab Initio* Total-Energy Calculations Using a Plane-Wave Basis Set. *Phys. Rev. B* **1996**, *54*, 11169−11186.
(28) Perdew, J. P.; Burke, K.; Ernzerhof, M. Generalized Gradient Approximation Made Simple. *Phys. Rev. Lett.* **1996**, *77*, 3865−3868.
(29) Methfessel, M.; Paxton, A. T. High-Precision Sampling for Brillouin-Zone Integration in Metals. *Phys. Rev. B* **1989**, *40*, 3616−3621.
(30) Momma, K.; Izumi, F. VESTA 3 for Three-Dimensional Visualization of Crystal, Volumetric and Morphology Data. *J. Appl. Crystallogr.* **2011**, *44*, 1272−1276.

https://doi.org/10.1021/acsomega.1c04730
ACS Omega 2021, 6, 33701−33707